

Approximation of reduced width amplitude and application to cluster decay width

Yoshiko Kanada-En'yo

Department of Physics, Kyoto University, Kyoto 606-8502, Japan

Tadahiro Suhara

Matsue College of Technology, Matsue 690-8518, Japan

Yasutaka Taniguchi

*Center for Computational Sciences, University of Tsukuba, Tsukuba 305-8571, Japan
Nihon Institute of Medical Science, Moroyama-machi, Iruma-gun, Saitama 350-0435, Japan*

We propose a simple method to approximately evaluate reduced width amplitude (RWA) of a two-body spinless cluster channel using the norm overlap with the Brink-Bloch cluster wave function at the channel radius. The applicability of the present approximation is tested for the $^{16}\text{O}+\alpha$ channel in ^{20}Ne as well as the $\alpha+\alpha$ channel in ^8Be . The approximation is found to be reasonable to evaluate the RWA for states near the threshold energy and it is useful to estimate the α -decay width of resonance states. The approximation is also applied to ^9Li , and the partial decay width of the $^6\text{He}(0_1^+)+t$ channel is discussed.

I. INTRODUCTION

In the recent experimental and theoretical studies, it has been revealed that a variety of cluster structures appear in various stable and unstable nuclei in a wide mass-number region (for instance, Refs. [1–4] and references therein). As predicted in Ikeda's threshold rule [5, 6], remarkable cluster structures with spatial development have been suggested in excited states near the threshold energy. Interestingly, in neutron-rich nuclei, various cluster states containing exotic clusters have been suggested: $\text{He}+\text{He}$ cluster states in Be isotopes [2, 3, 7–33], $^{10}\text{Be}+\alpha$ states in ^{14}C [34–38], $^{14}\text{C}+\alpha$ states in ^{18}O and their mirror states [39–48], $^{18}\text{O}+\alpha$ states in ^{22}Ne [46–53], $^9\text{Li}+^6\text{He}$ states in ^{15}B [18], $^6\text{He}+t$ states in ^9Li [54], and so on.

For direct evidence of clusters in nuclei, the cluster decay width is a probe to confirm the cluster structure in resonance states. Theoretically, conventional cluster models such as the resonating group method (RGM) [55, 56] and the generator coordinate method (GCM) [57, 58] have been applied to study typical cluster structures in light stable nuclei such as the $\alpha+\alpha$ structure in ^8Be and the $^{16}\text{O}+\alpha$ structure in ^{20}Ne , and they have succeeded to describe cluster decay widths of resonance states [6, 59–64].

As the variation of constituent clusters becomes richer in unstable nuclei than the well-known cluster structures in stable nuclei, conventional cluster models based on the assumption of specific clusters such as α and ^{16}O are no longer applicable for new cluster states having exotic clusters as t , ^6He , ^8He , ^{10}Be , ^{14}C , and ^{18}O . For such exotic clusters, it is important to take into account cluster polarization, breaking, and formation as well as effects of channel coupling. For cluster study of unstable nuclei, many extended frameworks such as antisymmetrized molecular dynamics (AMD) [3, 65–67] and fermionic molecular dynamics (FMD) methods [68–71], and extended cluster models of the stochastic variational method [16, 72], the GCM method, and the generalized two-center cluster model [20, 22] have been developed.

One of the advantages of the AMD method is that the framework does not rely on the assumption of any clusters. Nevertheless the model wave function can describe various cluster structures as well as one-center structures expressed by a shell-model configuration as the formation and dissociation of clusters are automatically obtained in the energy variation. The method has been applied to stable and unstable nuclei and proved to be useful for study of cluster structures in general nuclei. In spite of the flexibility of the AMD wave function, its application to cluster decay widths is very limited. One of the main origins for the difficulty is that internal wave functions of exotic clusters are generally more complicated than typical clusters which can be often expressed by a simple shell-model configuration. In such a case, it needs a large numerical cost to describe the details of asymptotic inter-cluster wave functions mainly because superposition of wave functions is needed in describing exotic clusters. The FMD framework, whose wave function is quite similar to the AMD one, has been applied to a scattering problem by Neff *et al.* [71], but, the application is limited only to very light nuclei. In many works of cluster structures with the AMD method, cluster resonance states are often described in a bound state approximation and their widths are hardly discussed.

Our aim is to estimate cluster decay widths by measuring the cluster probability at the surface for general A -body wave functions containing exotic clusters or non-cluster components. According to the R -matrix theory of nuclear reaction, the cluster decay width is given by the reduced width amplitude (RWA) at a channel radius where the interaction and the antisymmetrization effect of nucleons between clusters vanish. The method with the RWA is

often used to estimate the cluster decay width in traditional cluster models within a bound-state approximation. It means that if one has a reliable value of the RWA in an A -body wave function, it is able to estimate the cluster decay width following the RWA method as done in cluster models. However, to extract the RWA for exotic clusters from a total wave function, one may encounter another problem because it is not obvious how to separate the partial-wave inter-cluster wave function and cluster internal wave functions under the antisymmetrization operator of nucleons between clusters. Instead, it is easier to calculate the norm overlap of the total wave function with the reference cluster wave functions where clusters are localized around a certain position rather than to directly extract the RWA. Even for exotic clusters described by rather complicated configurations, the calculation of the norm overlap is usually feasible. In the region of our interest where the effect of antisymmetrization of nucleons between clusters is negligible, the norm overlap indicates the cluster probability at a certain channel radius and it should relate to the RWA.

In this paper, we propose a simple method to approximately calculate the RWA at the surface region using the norm overlap with the reference cluster wave function. To check the validity of the present approximation of the RWA, we compare the approximated RWA with the exact RWA in the well-known cluster states; $^{16}\text{O}+\alpha$ in ^{20}Ne and $\alpha+\alpha$ states in ^8Be in the traditional cluster-GCM calculations. We also make similar analysis for the ^{20}Ne wave functions with the mixing of non-cluster components obtained with the AMD method. We show the applicability of the present approximation to discuss the α -decay widths of cluster resonance states in ^{20}Ne and ^8Be . As an example of application to neutron-rich nuclei, we apply the present method to ^9Li and discuss the partial width of t decay from the $^6\text{He}+t$ cluster resonances suggested in the previous work in Ref. [54].

The paper is organized as follows; In the next section, we explain the conventional cluster-GCM model with Brink-Bloch (BB) cluster wave functions, and describe the RWA and its relation to the decay width in the cluster model. The method to approximately calculate the RWA is proposed in Sec. III. The AMD framework is briefly reviewed in Sec. IV. The application of the present method is demonstrated in Sec. V, and finally a summary and outlooks are given in Sec. VI.

II. CLUSTER WAVE FUNCTIONS AND REDUCED WIDTH AMPLITUDE

In this section, we review the traditional cluster-GCM model and the RWA. For more details, the reader is referred to the review article [64] and references therein.

A. BB cluster model and GCM wave functions

Let us consider a system composed of two spinless clusters C_1 and C_2 with mass numbers A_1 and A_2 , respectively. In the GCM of the C_1+C_2 cluster model, the total wave function can be expressed by the linear combination of BB cluster model wave functions [58].

A BB cluster model wave function of the two-cluster C_1+C_2 system with the relative position \mathbf{S} is expressed as

$$|\Phi_{\text{Brink-Bloch}}(\mathbf{S})\rangle = \left| \frac{1}{\sqrt{A!}} \mathcal{A} \left\{ \psi(C_1, \frac{-A_2}{A} \mathbf{S}) \psi(C_2, \frac{A_1}{A} \mathbf{S}) \right\} \right\rangle. \quad (1)$$

Here $\psi(C_i, \mathbf{S}_i)$ is the wave function of the C_i cluster localized around \mathbf{S}_i , and it is given by the harmonic oscillator (H.O.) shell model wave function with the shifted center at \mathbf{S}_i . We choose the same width of H.O. for C_1 and C_2 . We set the relative position \mathbf{S} on the z -axis $\mathbf{S} = (0, 0, S)$, and for simplicity, rewrite the BB wave function parametrized by the inter-cluster distance $|\mathbf{S}| = S$ as

$$|\Phi_{\text{BB}}(S)\rangle \equiv |\Phi_{\text{Brink-Bloch}}(\mathbf{S} = (0, 0, S))\rangle. \quad (2)$$

We define the normalized J^π -projected BB wave function,

$$|\Phi_{\text{BB}}^{J\pi}(S_k)\rangle \equiv \frac{1}{\sqrt{n_0^J(S_k)}} P_{00}^{J\pi} |\Phi_{\text{BB}}(S_k)\rangle, \quad (3)$$

$$P_{MK}^{J\pi} \equiv P^\pi P_{MK}^J \quad (4)$$

$$P^{\pi=\pm} = \frac{1 \pm P_r}{2} \quad (5)$$

$$P_{MK}^J = \frac{2J+1}{8\pi^2} \int d\Omega D_{MK}^{J*}(\Omega) R(\Omega). \quad (6)$$

P^π and P_{MK}^J are the parity and total angular-momentum (spin) projection operators. The BB wave function of two spinless clusters with $\mathbf{S} = (0, 0, S)$ is the $K = 0$ eigen state, and its J -projected state is the parity $\pi = (-1)^J$ eigen state where the inter-cluster wave function is projected onto the partial $l = J$ wave. The normalization factor $n_0^l(S_k)$ is chosen to be $n_0^l(S_k) = \langle \Phi_{\text{BB}}(S_k) | P_{00}^{J\pi} P_{00}^{J\pi} | \Phi_{\text{BB}}(S_k) \rangle$ so as to satisfy $|\Phi_{\text{BB}}^{J\pi}(S_k)|^2 = 1$.

The cluster-GCM wave function for a J^π state is given by the linear combination of the projected BB wave functions,

$$|\Phi_{\text{GCM}}\rangle = \sum_k c_k |\Phi_{\text{BB}}^{J\pi}(S_k)\rangle. \quad (7)$$

Coefficients c_k are determined by solving the discretized Hill-Wheeler equation which is equivalent to the diagonalization of the norm and Hamiltonian matrices. Here, the cluster-GCM wave function Φ_{GCM} is normalized as $\langle \Phi_{\text{GCM}} | \Phi_{\text{GCM}} \rangle = 1$. In $|\Phi_{\text{BB}}(S_k)\rangle$, the relative wave function between clusters is written by a localized Gaussian wave packet, and its partial wave expansion is given as follows.

$$|\Phi_{\text{BB}}(S_k)\rangle = |\frac{1}{\sqrt{A!}} \mathcal{A}\{\Gamma(\mathbf{r}, \mathbf{S} = (0, 0, S_k), \gamma) \phi(C_1) \phi(C_2) \phi_{\text{c.m.}}\}\rangle, \quad (8)$$

$$\Gamma(\mathbf{r}, \mathbf{S}, \gamma) = \left(\frac{2\gamma}{\pi}\right)^{3/4} e^{-\gamma(\mathbf{r}-\mathbf{S})^2} = \sum_l \Gamma_l(r, S, \gamma) \sum_m Y_{lm}(\hat{\mathbf{r}}) Y_{lm}^*(\hat{\mathbf{S}}), \quad (9)$$

$$\Gamma_l(r, S, \gamma) \equiv 4\pi \left(\frac{2\gamma}{\pi}\right)^{3/4} i_l(2\gamma S r) e^{-\gamma(r^2+S^2)}, \quad (10)$$

$$\gamma \equiv \frac{A_1 A_2}{A} \nu, \quad (11)$$

$$\phi_{\text{c.m.}} = \left(\frac{2A\nu}{\pi}\right) e^{-A\nu \mathbf{r}_G^2}, \quad (12)$$

where i_l is the modified spherical Bessel function, \mathbf{r} is the relative coordinate between centers of mass of clusters, $\phi(C_1)$ and $\phi(C_2)$ are internal wave functions of clusters \mathbf{r}_G is the center of mass coordinate and $\phi_{\text{c.m.}}$ is the wave function of the total center of mass motion (c.m.m.). ν is the width parameter for the H.O. for clusters, and relates to the width b of the H.O. as $\nu \equiv 1/2b^2$. Then, in the projected BB wave function $|\Phi_{\text{BB}}^{J\pi}(S_k)\rangle$, the radial part $\chi_l^{\text{BB}}(S_k; r)$ of the l -wave relative wave function is written with the function Γ_l ;

$$|\Phi_{\text{BB}}^{J\pi}(S_k)\rangle = |\frac{1}{\sqrt{A!}} \mathcal{A}\{\chi_l^{\text{BB}}(S_k; r) Y_{l0}(\hat{\mathbf{r}}) \phi(C_1) \phi(C_2) \phi_{\text{cm}}\}\rangle, \quad (13)$$

$$\chi_l^{\text{BB}}(S_k; r) = \frac{1}{\sqrt{n_0^l(S_k)}} \sqrt{\frac{2l+1}{4\pi}} \Gamma_l(r, S_k, \gamma). \quad (14)$$

Here the relation $Y_{l0}^*(\hat{\mathbf{S}}) = \sqrt{\frac{2l+1}{4\pi}}$ for $\mathbf{S} = (0, 0, S_k)$ is used.

Using $\chi_l^{\text{BB}}(S_k; r)$, the cluster-GCM wave function is also rewritten in the form consisting of the relative wave function, internal wave functions of clusters, and the c.m. wave function,

$$\Phi_{\text{GCM}} = \sum_k c_k |\Phi_{\text{BB}}^{J\pi}(S_k)\rangle = |\frac{1}{\sqrt{A!}} \mathcal{A}[\chi_l^{\text{GCM}}(r) Y_{l0}(\hat{\mathbf{r}}) \phi(C_1) \phi(C_2) \phi_{\text{c.m.}}]\rangle \quad (15)$$

$$\chi_l^{\text{GCM}}(r) = \sum_k c_k \chi_l^{\text{BB}}(S_k; r) \sum_k c_k \sqrt{\frac{2l+1}{4\pi}} \Gamma_l(r, S_k, \gamma). \quad (16)$$

B. Reduced width amplitude

For a wave function Ψ of the A -nucleon system, the RWA $ry_l(r)$ for the C_1+C_2 cluster channel is defined as

$$ry_l(r) \equiv r \sqrt{\frac{A!}{A_1! A_2!}} \langle Y_{l0}(\hat{\mathbf{r}}) \phi(C_1) \phi(C_2) | \Psi \rangle. \quad (17)$$

Here Ψ does not contain the c.m.m. $y_l(r)$ is regarded as the radial part of a relative wave function where the antisymmetrization effect is taken into account.

For a RGM-type cluster wave function of the C_1+C_2 system,

$$\Psi = \frac{1}{\sqrt{A!}} \mathcal{A} [\chi_l(r) Y_{l0}(\hat{r}) \phi(C_1) \phi(C_2)], \quad (18)$$

y_l is calculated by using the expansion of $\chi_l(r)$ with the orthonormal set $R_{nl}(r)$ of the radial wave functions of H.O. with the width parameter $b = 1/\sqrt{2\gamma}$ given by $\gamma = \nu A_1 A_2 / A$,

$$\chi_l(r) = \sum_n a_n R_{nl}(r), \quad (19)$$

$$a_n = \int r^2 dr R_{nl}(r) \chi_l(r), \quad (20)$$

$$y_l(r) = \sum_n a_n \mu_{nl} R_{nl}(r), \quad (21)$$

μ_{nl} is the eigen value of the RGM norm kernel [64]. We also define the function $u(r)$ as

$$u_l(r) = \sum_n a_n \sqrt{\mu_{nl}} R_{nl}(r). \quad (22)$$

For the normalized cluster wave function $\langle \Psi | \Psi \rangle = 1$, the function $u_l(r)$ also satisfies the normalization,

$$\int |u_l(r)|^2 r^2 dr = 1. \quad (23)$$

The spectroscopic factor S is defined by the RWA,

$$S = \int |y_l(r)|^2 r^2 dr. \quad (24)$$

Functions, $\chi_l(r)$, $y_l(r)$, and $u_l(r)$ are interpreted as inter-cluster wave functions, *i.e.*, the radial part of relative wave functions, but they are different in the treatment of the antisymmetrization effect between clusters. $\chi_l(r)$ is the relative wave function before antisymmetrization and can contain unphysical forbidden states with $\mu_{nl} = 0$. In the functions, $y_l(r)$ and $u_l(r)$, the antisymmetrization is taken into account and all forbidden states are excluded in both functions, but the treatment of partially allowed states with $\mu_{nl} \neq 1$ is different. All the functions $\chi_l(r)$, $y_l(r)$, and $u_l(r)$ have the same asymptotic behavior in the large r region where the antisymmetrization effect between clusters vanishes while they are different in the inner region where clusters largely overlap with each other and feel the strong antisymmetrization effect.

C. Inter-cluster wave functions for GCM and BB wave functions

For the cluster-GCM wave function, the inter-cluster wave functions $y_l^{\text{GCM}}(r)$ is calculated from the function $\chi_l^{\text{GCM}}(r)$,

$$\chi_l^{\text{GCM}}(r) = \sum_n a_n R_{nl}(r), \quad (25)$$

$$a_n = \int r^2 dr R_{nl}(r) \chi_l^{\text{GCM}}(r), \quad (26)$$

$$y_l^{\text{GCM}}(r) = \sum_n a_n \mu_{nl} R_{nl}(r). \quad (27)$$

$r y_l^{\text{GCM}}(r)$ is the RWA of the cluster-GCM wave function.

Also for the J^π -projected BB wave function $\Phi_{\text{BB}}^{J\pi}(S_k)$, we can define the antisymmetrized inter-cluster wave functions $y_l^{\text{BB}}(r)$ and $u_l^{\text{BB}}(r)$ from the non-antisymmetrized wave function $\chi_l^{\text{BB}}(r)$,

$$y_l^{\text{BB}}(S_k; r) = \sum_n a_n \mu_{nl} R_{nl}(r), \quad (28)$$

$$u_l^{\text{BB}}(S_k; r) = \sum_n a_n \sqrt{\mu_{nl}} R_{nl}(r), \quad (29)$$

$$a_n = \int r^2 dr R_{nl}(r) \chi_l^{\text{BB}}(S_k; r). \quad (30)$$

Here, the normalization $\int |u_l^{\text{BB}}(S_k; r)|^2 r^2 dr = 1$ is satisfied because of the condition $|\Phi_{\text{BB}}^{J\pi}(S_k)|^2 = 1$.

D. Antisymmetrization effect between clusters

A BB wave function is parametrized by the inter-cluster distance parameter S_k . The non-antisymmetrized wave function $\chi_l^{\text{BB}}(S_k; r)$ is the function localized around $r = S_k$. In case of a small S_k , clusters largely overlap with each other and the inter-cluster wave function is strongly affected by the antisymmetrization of nucleons between clusters. For such a small S_k , $\chi_l^{\text{BB}}(S_k; r)$ contains much component of unphysical forbidden states, which do not affect the total wave function $\Phi_{\text{BB}}^{J\pi}(S_k)$. Since the forbidden states are excluded in $u_l^{\text{BB}}(r)$ as well as $y_l^{\text{BB}}(r)$, the norm of the original function $\chi_l^{\text{BB}}(S_k; r)$ is usually larger than that of $u_l^{\text{BB}}(r)$. In other words, because of the antisymmetrization the norm of inter-cluster wave function $u_l^{\text{BB}}(r)$ is relatively small compared with the original one $\chi_l^{\text{BB}}(S_k; r)$. We call the ratio of norms

$$\mathcal{N}_l(S_k) \equiv \frac{\int |u_l^{\text{BB}}(r)|^2 r^2 dr}{\int |\chi_l^{\text{BB}}(S_k; r)|^2 r^2 dr} = \frac{1}{\int |\chi_l^{\text{BB}}(S_k; r)|^2 r^2 dr}, \quad (31)$$

“allowedness factor” which indicates the weakness of the antisymmetrization effect between clusters. In a BB wave function with an enough large S_k where the antisymmetrization effect between clusters is negligible, $\mathcal{N}_l(S_k) \simeq 1$. In such a case, the antisymmetrized inter-cluster wave functions $y_l^{\text{BB}}(S_k; r)$ and $u_l^{\text{BB}}(S_k; r)$ are consistent with the original non-antisymmetrized wave function $\chi_l^{\text{BB}}(S_k; r)$. In a small S_k limit, $\chi_l^{\text{BB}}(S_k; r)$ is dominated by unphysical forbidden states and the ratio of the norms for the physical inter-cluster wave function $\int |u_l^{\text{BB}}(r)|^2 r^2 dr$ to that for $\int |\chi_l^{\text{BB}}(S_k; r)|^2 r^2 dr$ goes to zero, *i.e.*, the allowedness factor $\mathcal{N}_l(S_k) \approx 0$ indicating the strong limit of the antisymmetrization effect.

Moreover, the relative wave function $\chi_l^{\text{BB}}(S_k; r)$ has a peak structure around $r = S_k$. It means that, for a large S_k , the function $r\chi_l^{\text{BB}}(S_k; r) \approx ry_l^{\text{BB}}(S_k; r) \approx ru_l^{\text{BB}}(S_k; r)$ is a localized function around $r = S_k$.

E. Decay width and RWA

For the α -decay width Γ_α , the reduced width $\gamma_\alpha^2(a)$ at the channel radius a is defined

$$\Gamma_\alpha = 2P_l(a)\gamma_\alpha^2(a), \quad (32)$$

$$P_l(a) = \frac{ka}{F_l^2(ka) + G_l^2(ka)}, \quad (33)$$

where F_l and G_l are the regular and irregular Coulomb functions, respectively, k is the momentum of inter-cluster motion in the asymptotic region, and mu is the reduced mass. A dimensionless reduced α -width $\theta_\alpha^2(a)$ defined by the ratio of the reduced α -width $\gamma_\alpha^2(a)$ to its Wigner limit $\gamma_W^2(a) = 3\hbar^2/2\mu a^2$,

$$\theta_\alpha^2(a) = \gamma_\alpha^2(a)/\gamma_W^2(a), \quad (34)$$

is a good measure to discuss the α -cluster probability at the surface. The experimental value of $\theta_\alpha^2(a)$ is deduced from the measured α -decay width Γ_α of the resonance states.

On the other hand, according to the R -matrix theory of nuclear reaction, the reduced width is approximately given by the RWA $ay_l(a)$ for the α cluster channel,

$$\gamma_\alpha^2(a) = \frac{\hbar^2}{2\mu a} [ay_l(a)]^2 \quad (35)$$

$$\theta_\alpha^2(a) = \frac{a}{3} [ay_l(a)]^2. \quad (36)$$

This approximation is good especially for narrow resonances. In the theoretical calculation using a bound state approximation, the above R -matrix based approximation is often used to estimate the width from the calculated RWA $ay_l(a)$.

III. APPROXIMATED RWA

As mentioned above, the partial decay width can be estimated using the RWA $ry_l(r)$ at a channel radius $r = a$ with the relation given in Eq. (35) based on the R -matrix theory. Our aim here is to approximately evaluate the RWA $ry_l(r)$ at a certain channel radius for cluster-GCM wave functions Φ_{GCM} or more general A -body wave functions Φ having

cluster breaking components in order to estimate the partial width of cluster decay from resonance states. In general, clusters, C_1 and C_2 , are not shell-closed clusters and they have more complicated configurations than shell-closed nuclei. If clusters are deformed and their intrinsic wave functions are not spin-parity eigen wave functions, spin-parity projections of subsystems (clusters) are needed to calculate exact RWA and it usually enlarges the numerical cost. Moreover, it is not necessarily easy to solve the eigen value problem of the RGM norm kernel for the C_1+C_2 channel except for the case of simple clusters.

Alternatively, we propose a method to calculate an approximated value of the RWA $ay_l(a)$ using the simple overlap norm of Φ with a single BB cluster wave function parametrized by $S_k = a$. The region for the channel radius a of our interest is the surface region where the inter-cluster distance is large enough to ignore the antisymmetrization effect of nucleons between clusters. Let us consider the projected BB wave function $\Phi_{\text{BB}}^{J\pi}(S_k)$ with $S_k = a$ which is localized around the channel radius a . The overlap of Φ with $\Phi_{\text{BB}}^{J\pi}(S_k)$ can be calculated as the norm overlap of antisymmetrized A -body wave functions. It is also given by the overlap of the inter-cluster wave functions $u_l(r)$ for Φ and $u_l^{\text{BB}}(r)$ for $\Phi_{\text{BB}}^{J\pi}$,

$$|\langle \Phi | \Phi_{\text{BB}}^{J\pi}(S_k) \rangle| = |\langle ru_l(r) | ru_l^{\text{BB}}(S_k; r) \rangle|. \quad (37)$$

Here we define

$$\langle f(r) | g(r) \rangle \equiv \int_0^\infty f^*(r) g(r) dr. \quad (38)$$

As mentioned before, in the region around a where the antisymmetrization effect between clusters is negligible, $\chi(r) \approx y_l(r) \approx u_l(r)$ for Φ , and also $\chi_l^{\text{BB}}(S_k; r) \approx y_l^{\text{BB}}(S_k; r) \approx u_l^{\text{BB}}(S_k; r)$ for $\Phi_{\text{BB}}^{J\pi}(S_k)$. Moreover, for simplicity, we approximate the inter-cluster wave function $\chi_l^{\text{BB}}(S_k; r)$ for $\Phi_{\text{BB}}^{J\pi}(S_k)$ with a Gaussian form,

$$r\chi_l^{\text{BB}}(S_k; r) \approx \left(\frac{2\gamma}{\pi}\right)^{1/4} e^{-\gamma(r-S_k)^2} \equiv \mathcal{X}^G(S_k; r). \quad (39)$$

Namely, the inter-cluster wave function for $\Phi_{\text{BB}}^{J\pi}(S_k)$ is localized around $r = S_k$ with the width $2\sqrt{\gamma}$. Let us consider here to measure the unknown RWA $ry_l(r) \approx ru_l(r)$ with the localized reference function $\mathcal{X}^G(S_k; r) \approx ru_l^{\text{BB}}(S_k; r)$ using the equation (37),

$$|\langle \Phi | \Phi_{\text{BB}}^{J\pi}(S_k) \rangle| = |\langle ru_l(r) | ru_l^{\text{BB}}(S_k; r) \rangle| \approx \langle ry_l(r) | \mathcal{X}^G(S_k; r) \rangle. \quad (40)$$

We assume that the RWA $ry_l(r)$ for the realistic wave function Φ is a gradually changing function compared with the localized reference function $\mathcal{X}^G(S_k = a; r)$ and it can be approximated to be constant $ay(a)$ at least in the region around $S_k = a$ with the width $2\sqrt{\gamma}$ where $\mathcal{X}^G(S_k = a; r)$ gives a finite contribution to the integrated value $\langle ry_l(r) | \mathcal{X}^G(S_k; r) \rangle$. In this assumption, the overlap is approximately given as

$$\langle ry_l(r) | \mathcal{X}^G(S_k = a; r) \rangle \approx ay(a) \int \mathcal{X}^G(S_k = a; r) dr = ay(a) \sqrt{2} \left(\frac{2\gamma}{\pi}\right)^{-1/4}. \quad (41)$$

It means that the norm overlap with $\Phi_{\text{BB}}^{J\pi}(S_k = a)$ relates to the RWA $ay_l(a)$ and we obtain the following approximation for the RWA

$$|ay_l(a)| \approx \frac{1}{\sqrt{2}} \left(\frac{2\gamma}{\pi}\right)^{1/4} |\langle \Phi | \Phi_{\text{BB}}^{J\pi}(S_k = a) \rangle| \equiv ay^{\text{app}}(a). \quad (42)$$

This approximation works reasonably for the tail part of the RWA of cluster states near the threshold energy because the inter-cluster wave function has an asymptotic tail determined by the energy measured from the threshold. If $ry_l(r)$ is a rapidly changing function, the approximated function $ry^{\text{app}}(r)$ corresponds to a smeared function with the resolution $2\sqrt{\gamma}$ and $ay^{\text{app}}(a)$ indicates the mean value of $ry_l(r)$ around $r = a$. Moreover, the approximation is not valid in the small a region with the strong antisymmetrization effect. However, for the present aim to estimate decay width of resonances using the approximated RWA, we can reasonably approximate the RWA with the present method as shown later.

IV. AMD METHOD

The AMD method is useful to describe the formation and breaking of clusters as well as shell-model states with non-cluster structure. The applicability of the AMD method to stable and unstable nuclei have been proved, for example, in Refs. [3, 67]. For the detailed formulation of the AMD, the reader is referred to those references.

A. Formulation of AMD(VAP)

An AMD wave function of an A -nucleon system is given by a Slater determinant of Gaussian wave packets;

$$\Phi_{\text{AMD}}(\mathbf{Z}) = \frac{1}{\sqrt{A!}} \mathcal{A}\{\varphi_1, \varphi_2, \dots, \varphi_A\}, \quad (43)$$

$$\varphi_i = \phi_{\mathbf{X}_i} \sigma_i \tau_i, \quad (44)$$

$$\phi_{\mathbf{X}_i}(\mathbf{r}_j) = \left(\frac{2\nu}{\pi}\right)^{4/3} \exp\left\{-\nu\left(\mathbf{r}_j - \frac{\mathbf{X}_i}{\sqrt{\nu}}\right)^2\right\}, \quad (45)$$

$$\sigma_i = \left(\frac{1}{2} + \xi_i\right)\sigma_{\uparrow} + \left(\frac{1}{2} - \xi_i\right)\sigma_{\downarrow}. \quad (46)$$

$\phi_{\mathbf{X}_i}$ and σ_i are spatial and spin functions of the i th single-particle wave function, and τ_i is the isospin function fixed to be up (proton) or down (neutron). Accordingly, an AMD wave function is expressed by a set of variational parameters, $\mathbf{Z} \equiv \{\mathbf{X}_1, \mathbf{X}_2, \dots, \mathbf{X}_A, \xi_1, \xi_2, \dots, \xi_A\}$. The width parameter ν is chosen to be a common value for all nucleons.

The energy variation after spin and parity projections (VAP) is performed to get the AMD wave function for the lowest J^π state. The parameters \mathbf{X}_i and ξ_i ($i = 1 \sim A$) are varied to minimize the expectation value of the Hamiltonian, $\langle \Phi | H | \Phi \rangle / \langle \Phi | \Phi \rangle$, with respect to the spin-parity eigen wave function projected from an AMD wave function; $\Phi = P_{MK}^{J^\pi} \Phi_{\text{AMD}}(\mathbf{Z})$.

In the AMD model space, all single-nucleon wave functions are treated as independent Gaussian wave packets, and cluster formation and breaking are described by spacial configurations of Gaussian centers, \mathbf{X}_i . If we choose a specific set of the parameters $\{\mathbf{Z}\}$, the AMD wave function can be equivalent to a BB wave function. For instance, the $\alpha + \alpha$ BB wave function with \mathbf{S}_k is expressed by the AMD wave function by taking $\mathbf{X}_1 = \dots = \mathbf{X}_4 = \mathbf{S}_k/2$ and $\mathbf{X}_5 = \dots = \mathbf{X}_8 = -\mathbf{S}_k/2$ for spin-up and down protons and neutrons. Similarly, it is also able to express a $^{16}\text{O} + \alpha$ BB wave function with an AMD wave function.

B. Hybrid model of AMD(VAP)+cluster

In a single AMD wave function, which is based on a single Slater determinant, the inter-cluster wave function does not have the correct asymptotic behavior. However, in a realistic cluster state near the threshold energy, the inter-cluster wave function should have an outer tail whose asymptotic behavior is determined by the α -decay energy. To describe the detailed behavior of the outer tail, we perform the hybrid calculation by superposing the AMD(VAP) wave functions and $^{16}\text{O} + \alpha$ cluster BB wave functions as done in $^{16}\text{O} + ^{16}\text{O}$ cluster states in ^{32}S by Kimura *et al.* [73].

In the hybrid calculation, the wave function for the J^π state is written by superposing the AMD wave functions $\Phi_{\text{AMD}}(\mathbf{Z}^{J^\pi})$ obtained by VAP for various J^π states and the BB wave functions,

$$|\Phi\rangle = \sum_{J'} c(J') |P_{MK}^{J^\pi} \Phi_{\text{AMD}}(\mathbf{Z}^{J^\pi})\rangle + \sum_k c(k) |\Phi_{\text{BB}}^{J^\pi}(S_k)\rangle, \quad (47)$$

where the coefficients $c(J')$ and $c(k)$ are determined by the diagonalization of the norm and Hamiltonian matrices. $K = 0$ is chosen in the present calculation of ^{20}Ne .

C. Projection to cluster model space

For a general microscopic A -body wave function Φ of a spin and parity J^π eigen state, we can extract the cluster components of Φ when the c.m.m. of Φ is separable. The AMD wave function satisfies this condition.

From a set of the J^π -projected BB wave functions, $|\Phi_{\text{BB}}^{J^\pi}(S_k)\rangle$ ($k = 1, \dots, k_{\text{max}}$), an orthonormal set of wave functions, $|\Phi_m^{\text{cluster}}\rangle$ ($m = 1, \dots, k_{\text{max}}$), is constructed. Here Φ_m^{cluster} is given by the linear combination of the basis wave functions $\Phi_{\text{BB}}^{J^\pi}(S_k)$ so as to satisfy the orthonormality $\langle \Phi_m^{\text{cluster}} | \Phi_n^{\text{cluster}} \rangle = \delta_{mn}$. By using this orthonormal set of cluster wave functions, the projection operator P^{cluster} on to the model space of cluster wave functions is defined as

$$P^{\text{cluster}} \equiv \sum_m |\Phi_m^{\text{cluster}}\rangle \langle \Phi_m^{\text{cluster}}| \quad (48)$$

The cluster component in a general wave function Φ is given by the expectation value of the projection operator

$$\mathcal{P}^{\text{cluster}} \equiv \langle \Phi | P^{\text{cluster}} | \Phi \rangle. \quad (49)$$

For a single-channel cluster-GCM wave function, the cluster component $\mathcal{P}^{\text{cluster}} = 1$, while if Φ contains non-cluster components it is smaller than 1. The inter-cluster wave functions $\chi_l(r)$, $y_l(r)$ and $u_l(r)$ for the general wave function Φ can be calculated by projecting it onto the cluster model space expressed by the linear combination of the BB wave functions. For a normalized wave function Φ , the cluster component $\mathcal{P}^{\text{cluster}}$ can be also given in terms of the norm of the inter-cluster wave function $u_l(r)$ as

$$\mathcal{P}^{\text{cluster}} = \langle ru_l(r) | ru_l(r) \rangle = \int |u_l(r)|^2 r^2 dr. \quad (50)$$

V. APPLICATION OF THE APPROXIMATED RWA

We check the validity of the approximated RWA defined in (42) for $^{16}\text{O}+\alpha$ and $\alpha+\alpha$ systems by comparing the approximated RWA with the exact value. We then apply the present method to ^9Li and discuss the partial decay width of the $^6\text{He}(0_1^+)+t$ channel for excited states of ^9Li .

A. RWA in ^{20}Ne

In ^{20}Ne , the ground band ($K^\pi = 0_1^+$), the $K^\pi = 0^-$ band, and the higher-nodal $K^\pi = 0^+$ band starting from the $J^\pi = 0_4^+$ state are considered to be $^{16}\text{O}+\alpha$ cluster states because they are described well with $^{16}\text{O}+\alpha$ cluster models except for the energy position of the 8^+ state in the ground band. For the $^{16}\text{O}+\alpha$ cluster states, it is rather easy to calculate the exact RWA using the eigen values μ_{nl} of the RGM norm kernel because both clusters are shell-closed nuclei and their wave functions are given by simple H.O. configurations.

As the first test to check the present method of the approximated RWA, we calculate the approximated values $ry_l^{\text{app}}(r)$ for the $^{16}\text{O}+\alpha$ cluster-GCM wave function and compare them with the exact RWA. We obtain the wave function Φ^{GCM} for the ground and excited states of ^{20}Ne with the $^{16}\text{O}+\alpha$ cluster-GCM calculation. The adopted effective interaction is Volkov No.2 with $m = 0.62$ [74]. The width parameter $\nu = 0.16 \text{ fm}^{-2}$ is used for both ^{16}O and α clusters. Those interaction parameters and the width parameter are the same as those used in the preceding study of ^{20}Ne with the RGM by Matsuse *et al.* [63]. The parameter set reproduces well the ground-band energy spectra measured from the threshold energy as well as the root-mean-square radius of ^{16}O . As the basis wave functions of the cluster-GCM calculation, ten BB wave functions with the $^{16}\text{O}-\alpha$ distance $S_k = 1, 2, \dots, 10 \text{ fm}$ are adopted. It corresponds to a bound state approximation.

As an another test, we also do the similar analysis of the RWA using AMD wave functions of ^{20}Ne . It is a test to check the applicability of the method for the case that the system is not a pure cluster state because the AMD wave function can contain non-cluster components as well as the cluster component. We perform the AMD(VAP) calculation to obtain the optimum solution of the AMD wave functions for the $J^\pi = 0^+, 2^+, \dots, 8^+$ states in the ground band of ^{20}Ne . As for the effective interaction, Volkov No.2 with $m = 0.66$ supplemented by the spin-orbit force of the G3RS [75] with the strength $u_I = -u_{II} = 2400 \text{ MeV}$ is chosen so as to reproduce the ground band spectra measured from the threshold energy of the H.O. shell-closed ^{16}O and α clusters. In the AMD(VAP) calculation, the larger Majorana parameter m than that used in the cluster-GCM calculation is needed to avoid the overbinding problem because the extra energy is gained by the spin-orbit interaction and the cluster dissociation in the AMD(VAP) calculation. We also perform the hybrid calculation of AMD(VAP)+cluster by superposing AMD(VAP) wave functions and $^{16}\text{O}+\alpha$ cluster BB wave functions using the same interaction.

The calculated energy levels measured from the $^{16}\text{O}+\alpha$ threshold are shown in Fig. 1 compared with the experimental energy levels of the ground, the $K^\pi = 0^-$, and the higher-nodal(hn) $K^\pi = 0^+$ bands. The $J^\pi = 0_2^+, 2_2^+$, and 4_2^+ states obtained with the cluster-GCM calculation correspond to the higher-nodal band members, $0_{\text{hn}}^+, 2_{\text{hn}}^+$, and 4_{hn}^+ starting from the 0_4^+ state in the experimental data. It should be commented that the experimental 0_2^+ and 0_3^+ states can not be described within $^{16}\text{O}+\alpha$ cluster models because they are not simple $^{16}\text{O}+\alpha$ cluster states. The cluster-GCM calculation shows reasonable results for the energy levels except for the 6^+-8^+ level spacing as already shown in preceding works with $^{16}\text{O}+\alpha$ cluster models [61, 63]. The AMD(VAP) and hybrid calculations reproduce the ground band spectra. In particular, the small level spacing between 6^+ and 8^+ states is described well by the cluster breaking component in the 8^+ state at the band terminal consistently with the results of the cranking AMD calculation [65].

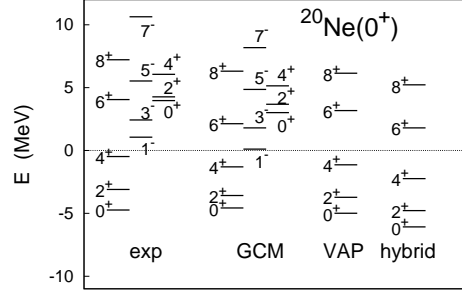


FIG. 1: Energies of the ground and excited states of ^{20}Ne obtained with the cluster-GCM, AMD(VAP), and the hybrid(AMD+cluster) calculations. The energies measured from the $^{16}\text{O}+\alpha$ threshold energy are compared with the experimental data [76]. The adopted effective interaction is Volkov No.2 with $m = 0.62$ for for cluster-GCM, and that with $m = 0.66$ supplemented by the spin-orbit term of the G3RS force with the strength $u_I = -u_{II} = 2400$ MeV for the AMD(VAP) and the hybrid calculations.

We first discuss the results of the cluster-GCM calculation. In Figs. 2, 3, and 4, the approximated RWA $ay_l^{\text{app}}(a)$ for Φ^{GCM} are compared with the exact values of $ay_l(a)$. The approximated RWA reasonably agrees with $ay_l(a)$ for bound states and resonance states in the region outer than the surface peak. The 6_2^+ and 8_2^+ states obtained by the cluster-GCM calculation have a feature of non-resonant continuum states, for which the approximation also works in the outer region.

In the small r region, the method of the approximated RWA does not work because the antisymmetrization effect of nucleons between clusters is rather strong and the norm overlap with a BB wave function does not directly indicate the α cluster probability at the certain position. We can judge the strength of the antisymmetrization effect using the allowedness factor $\mathcal{N}_l(S_k)$ shown in Figs. 2, 3, and 4. In the present result, it is found that the approximated RWA is not reliable for a small channel radius $S_k = a$ with $\mathcal{N}_l(S_k) < 0.4$ because of the strong antisymmetrization effect. To reject the unreliable region with the strong antisymmetrization effect, we put a more severe condition $\mathcal{N}_l(S_k) \geq 0.6$ as the applicable region because the agreement of $ry_l^{\text{app}}(r)$ to $ry_l(r)$ is rather well in the outside of the surface peak. Moreover, when the RWA is much smaller than the peak amplitude, the error becomes large even in the long distance tail part. Therefore, we reject $ry_l^{\text{app}}(r)$ if it is less than a half of the maximum amplitude in the applicable region. When the RWA has a broad peak in the applicable region, the channel radius a should be chosen around the peak position as shown in the result for higher-nodal band members, 0_2^+ , 2_2^+ , and 4_2^+ states.

TABLE I: Ratios $ay_l^{\text{app}}(a)/ry_l(a)$ of the approximated RWA to the exact RWA of the cluster-GCM calculation of ^{20}Ne . The channel radii $a = 5$ and 6 fm are chosen for the $K^\pi = 0_1^+$ and $K^\pi = 0^-$ bands except for the $J^\pi = 8_1^+$ state, and $a = 6$ and 7 fm for the higher-nodal $K^\pi = 0^+$ band.)

	$a = 4$	$a = 5$	$a = 6$	$a = 7$
$^{20}\text{Ne}(0_1^+)$		0.91	1.16	
$^{20}\text{Ne}(2_1^+)$		0.92	1.17	
$^{20}\text{Ne}(4_1^+)$		0.93	1.18	
$^{20}\text{Ne}(6_1^+)$		0.95	1.21	
$^{20}\text{Ne}(8_1^+)$	0.92	0.98		
$^{20}\text{Ne}(1_1^-)$		0.88	0.94	
$^{20}\text{Ne}(3_1^-)$		0.89	0.94	
$^{20}\text{Ne}(5_1^-)$		0.91	0.96	
$^{20}\text{Ne}(7_1^-)$		0.89	0.91	
$^{20}\text{Ne}(0_2^+)$			0.85	0.93
$^{20}\text{Ne}(2_2^+)$			0.87	0.94
$^{20}\text{Ne}(4_2^+)$			0.94	0.98

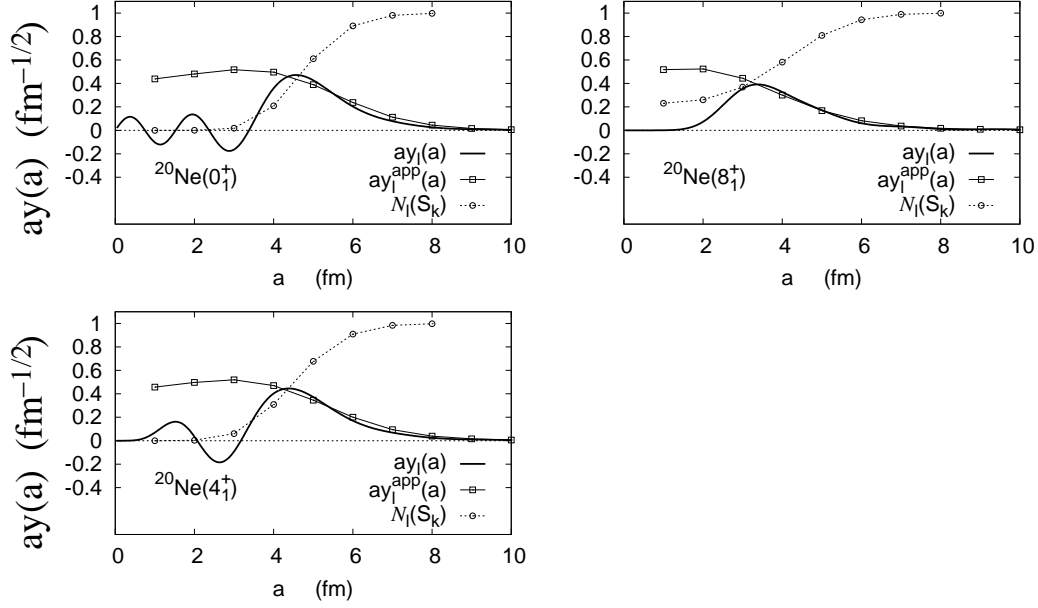


FIG. 2: The approximated RWA $ay_l^{\text{app}}(a)$ and the exact $ry_l(a)$ of the $^{16}\text{O}+\alpha$ channel for the $J^\pi = 0^+, 4^+, \text{ and } 8^+$ states in the ground band of ^{20}Ne obtained by the cluster-GCM calculation. The allowedness factor $\mathcal{N}_l(S_k = a)$, which indicates the weakness of the antisymmetrization effect of nucleons between clusters, in the projected BB wave function $\Phi_{\text{BB}}^{J^\pi}(S_k)$ is also shown.

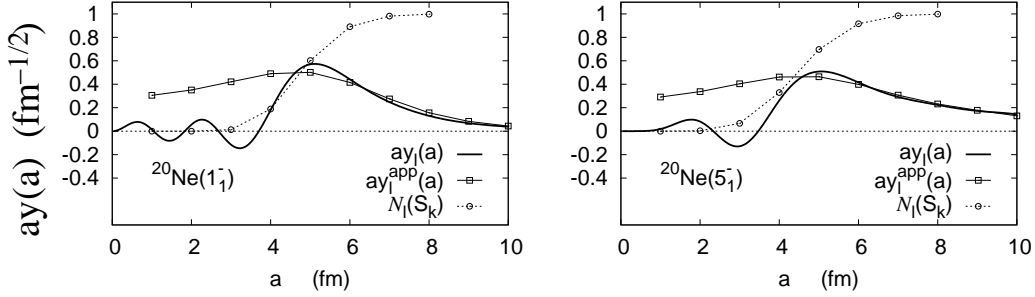


FIG. 3: Same as Fig. 2 but for the $J^\pi = 1^-$ and 5^- states in the $K^\pi = 0^-$ band of ^{20}Ne .

The ratios $y_l^{\text{app}}(r)/y_l(r)$ of the approximated RWA to the exact RWA are listed in Table I. For the $K^\pi = 0_1^+$ and $K^\pi = 0^-$ band members except for the $J^\pi = 8_1^+$ state, the channel radii $a = 5$ and 6 fm are chosen because the amplitude in the applicable region satisfying the condition $\mathcal{N}_l(S_k) \geq 0.6$ is maximum at $a = 5$ fm. For the $J^\pi = 8_1^+$ state, the applicable region is $a \geq 4$ fm and the amplitude at $a = 6$ fm is much smaller than the maximum amplitude at $a = 4$ fm, and therefore we choose the channel radii $a = 4$ and 5 fm. For the higher-nodal $K^\pi = 0^+$ band, we choose larger channel radii $a = 6$ and 7 fm as the peak position of the RWA shifts to the outer region around $a = 7-8$ fm. With the criterion that the allowedness factor should be $\mathcal{N}_l(S_k) \geq 0.6$ and the channel radius near the peak position should be chosen, we get good approximation of the approximated RWA with the exact value within about 20% error.

We also check the approximation of the RWA for the AMD(VAP) wave functions and the hybrid AMD(VAP)+cluster wave functions. In the result for the AMD(VAP) wave functions shown in Fig. 5, the approximation is not as good as the case of the cluster-GCM wave functions. As mentioned before, the AMD(VAP) wave function is the spin-parity eigen function projected from a single AMD wave function, and its inter-cluster wave function has a rapidly damping tail inconsistently with the correct asymptotic behavior. For such the localized function, the approximation does not work so well. Instead, $ry_l^{\text{app}}(r)$ corresponds to a smeared function of the exact $ry_l(r)$. However, in the realistic situation, the inter-cluster wave function has an outer tail with the correct asymptotic behavior determined by the

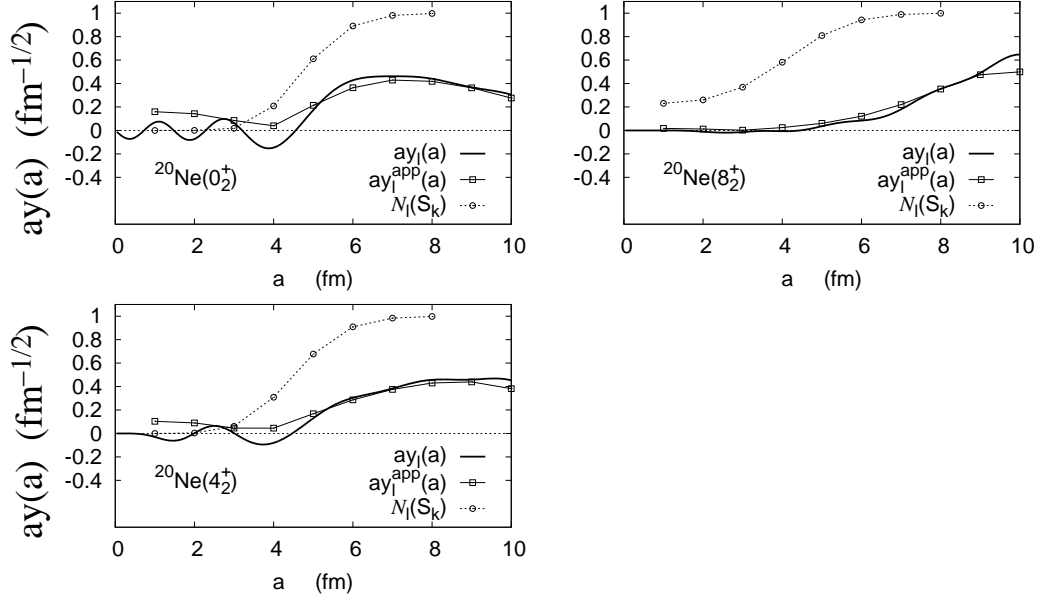


FIG. 4: Same as Fig. 2 but for the $J^\pi = 0^+, 4^+,$ and 8^+ states in the higher-nodal $K^\pi = 0^+$ band of ^{20}Ne .

α -decay energy, it should be a gradually changing function for states near the threshold energy. To describe the detailed behavior of the outer tail, we perform the hybrid calculation by superposing the AMD(VAP) wave functions for the $J^\pi = 0^+, 2^+, 4^+, 6^+,$ and 8^+ states and $^{16}\text{O} + \alpha$ cluster BB wave functions. In the hybrid wave functions, the tail parts of the inter-cluster wave functions are improved and it is found that the RWA $ay_l(a)$ can be approximated by $ay_l^{\text{app}}(a)$ in the outer region as shown in Fig. 6.

It should be noted that the cluster component $\mathcal{P}^{\text{cluster}}$ in the hybrid wave functions is less than 1 because of the cluster breaking component in the AMD(VAP) wave functions. The reduction effect of the cluster component to the RWA is properly taken into account in the present approximation of the RWA through the norm overlap. The reduction is significant in the band terminal state $^{20}\text{Ne}(8_1^+)$ with $\mathcal{P}^{\text{cluster}} \sim 0.44$ in the hybrid calculation.

B. α decay widths of ^{20}Ne

Using the relation (35) based on the R -matrix theory of nuclear reaction, we can evaluate the dimensionless reduced width $\theta_\alpha^2(a)$ for the α decay with the calculated RWA, $ay_l(a)$ and $ay_l^{\text{app}}(a)$.

The theoretical values of $\theta_\alpha^2(a)$ calculated with the approximated RWA $ay_l^{\text{app}}(a)$ are shown in table II compared with those obtained with the exact RWA $ay_l(a)$. We choose the channel radius $a = 5$ and 6 fm for the ground band and $K^\pi = 0^-$ band members, and $a = 6$ and 7 fm for the higher-nodal states. In both cases of the cluster-GCM and the hybrid wave functions, $\theta_\alpha^2(a)$ from $ay_l^{\text{app}}(a)$ agrees with that from $ay_l(a)$ within 20 – 30% error. It means that the present approximation for the RWA is practically useful to evaluate the correct RWA at the channel radius in the region of our interest to estimate the α -decay width.

In table III, we list the experimental $\theta_\alpha^2(a)$ for resonance states obtained with the observed decay width Γ_α . We also show the theoretical $\theta_\alpha^2(a)$ of the RGM calculation in Ref. [63] and the GCM calculation in Ref. [61]. The GCM calculation in Ref. [61] is a bound state approximation and the relation (35) of the α -decay width and the RWA is used. The calculation is quite similar to the present calculation but the interaction used in Ref. [61] is different from the present one. In the RGM calculation in Ref. [63], the $\theta_\alpha^2(a)$ is evaluated by the phase shift analysis by solving the scattering problem.

The present result of $\theta_\alpha^2(a)$ obtained by the cluster-GCM calculation is similar to those of Refs. [61, 63]. The theoretical $\theta_\alpha^2(a)$ is comparable to the experimental data. There are significant disagreements between calculated values and experimental ones for the decay width of $^{20}\text{Ne}(8_1^+)$ and $^{20}\text{Ne}(7^-)$. For those states, the cluster-GCM calculation overestimates the experimental α -decay width by a factor 2 – 5 as well as the cluster-model calculations in Refs. [61, 63]. The result is improved in the hybrid calculation where the cluster component $\mathcal{P}^{\text{cluster}}$ of $^{20}\text{Ne}(8_1^+)$ reduces to $\mathcal{P}^{\text{cluster}} \sim 0.4$ because of the mixing of the cluster breaking component.

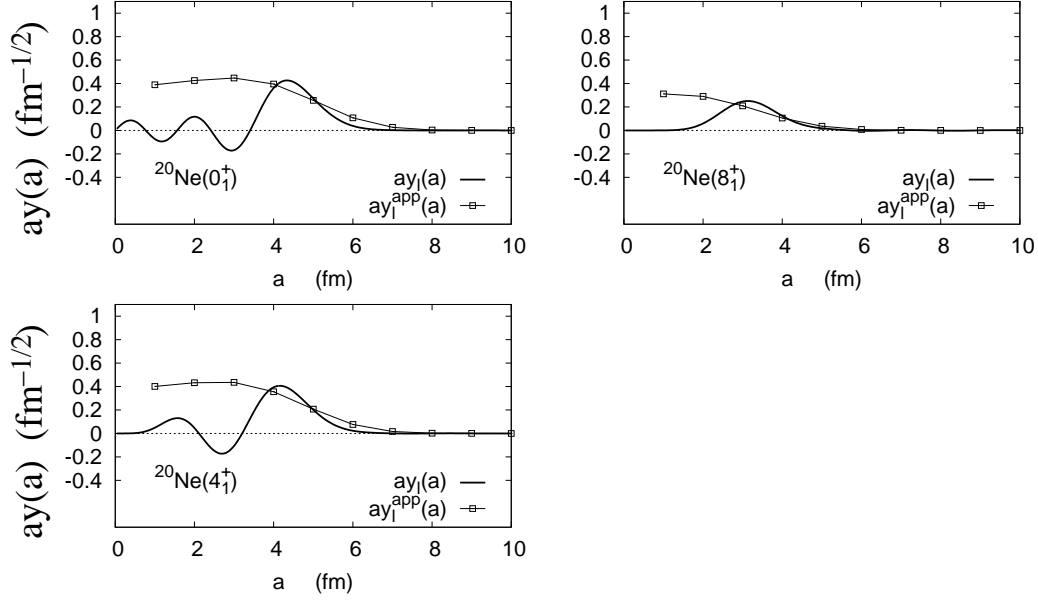


FIG. 5: The approximated RWA $ay_l^{app}(a)$ and the exact RWA $ry_l(a)$ of the $^{16}\text{O}+\alpha$ channel for the $J^\pi = 0^+, 4^+, \text{ and } 8^+$ states in the ground band of ^{20}Ne obtained by the AMD(VAP) calculation.

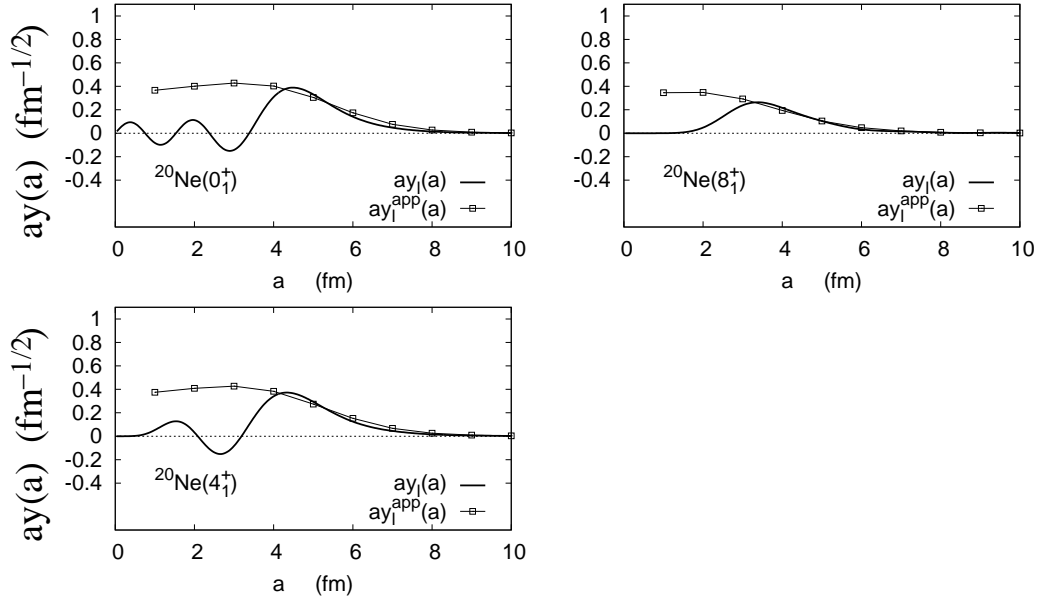


FIG. 6: Same as Fig. 5 but for the hybrid calculation of the AMD(VAP)+cluster wave functions.

According to the R -matrix theory, the relation (35) of the reduced width and the RWA is a good approximation, especially, for narrow resonances. However, strictly speaking, it is not necessarily good for broad resonances. Nevertheless, the present result using (35) in the bound state approximation shows reasonable values of the α -decay width even for such broad resonances as $^{20}\text{Ne}(0_{\text{hn}}^+)$ and $^{20}\text{Ne}(2_{\text{hn}}^+)$. It may suggest that the bound state approximation is still useful for a rough estimation of cluster-decay width.

In the present result of ^{20}Ne it is found that the $ay_l^{app}(a)$ is a good approximation of the RWA at the surface region and it is useful for our aim to give qualitative discussion of the α -decay width.

TABLE II: Dimensionless reduced width $\theta^2(a)$ of the $^{16}\text{O}+\alpha$ channel calculated with the relation 35 using the exact RWA $ay_l(a)$ and the approximated one $ay_l^{\text{app}}(a)$ for ^{20}Ne obtained by the cluster-GCM calculation. The channel radii $a = 5$ and $a = 6$ fm are chosen for the ground band and $K^\pi = 0^-$ band members, and $a = 6$ and $a = 7$ fm are chosen for the higher-nodal states. The energy E (MeV) measured from the threshold is also listed.

cluster-GCM					
	E	$\theta^2(a)$		$\theta^2(a)$	
		exact		approx.	
		$a = 5$	$a = 6$	$a = 5$	$a = 6$
$^{20}\text{Ne}(0_1^+)$	-4.57	0.30	0.08	0.25	0.11
$^{20}\text{Ne}(2_1^+)$	-3.58	0.28	0.08	0.24	0.10
$^{20}\text{Ne}(4_1^+)$	-1.30	0.23	0.06	0.20	0.08
$^{20}\text{Ne}(6_1^+)$	2.13	0.15	0.03	0.13	0.05
$^{20}\text{Ne}(8_1^+)$	6.31	0.05	0.007	0.05	
$^{20}\text{Ne}(1_1^-)$	0.11	0.54	0.39	0.42	0.35
$^{20}\text{Ne}(3_1^-)$	1.80	0.52	0.38	0.41	0.34
$^{20}\text{Ne}(5_1^-)$	4.86	0.43	0.35	0.36	0.32
$^{20}\text{Ne}(7_1^-)$	8.18	0.39	0.26	0.31	0.22
		$a = 6$	$a = 7$	$a = 6$	$a = 7$
$^{20}\text{Ne}(0_2^+)$	3.01	0.37	0.50	0.26	0.43
$^{20}\text{Ne}(2_2^+)$	3.68	0.31	0.46	0.24	0.41
$^{20}\text{Ne}(4_2^+)$	5.14	0.18	0.34	0.16	0.33
hybrid AMD(VAP)+cluster					
	E	$\theta^2(a)$		$\theta^2(a)$	
		exact		approx.	
		$a = 5$	$a = 6$	$a = 5$	$a = 6$
$^{20}\text{Ne}(0_1^+)$	-6.08	0.18	0.040	0.15	0.061
$^{20}\text{Ne}(2_1^+)$	-4.79	0.18	0.039	0.15	0.059
$^{20}\text{Ne}(4_1^+)$	-2.24	0.14	0.031	0.13	0.047
$^{20}\text{Ne}(6_1^+)$	1.79	0.094	0.020	0.085	0.029
$^{20}\text{Ne}(8_1^+)$	5.22	0.018	0.002	0.018	

C. ^8Be

We perform the similar analysis for $^8\text{Be}(0_1^+)$ and $^8\text{Be}(2_1^+)$ obtained by the $\alpha+\alpha$ cluster-GCM calculation and check the applicability of the approximated RWA. The Volkov No.2 interaction with $m = 0.60$ is used to reproduce the energy E of $^8\text{Be}(0_1^+)$. For the basis wave functions in the cluster-GCM calculation, the $\alpha+\alpha$ BB wave functions with $S_k = 1, 2, \dots, 10$ fm are used, and the width parameter $\nu = 0.25 \text{ fm}^{-2}$ is chosen for the α cluster wave function. The approximated RWA $ry_l^{\text{app}}(r)$ is shown in Fig. 7 compared with the correct RWA. It is shown that $ry_l^{\text{app}}(r)$ is a good approximation to describe the RWA of the tail part because $^8\text{Be}(0_1^+)$ and $^8\text{Be}(2_1^+)$ are quasi-bound $\alpha+\alpha$ states having the long tail of the inter-cluster wave function. In table IV, we show the dimensionless reduced α -decay width $\theta^2(a)$ of ^8Be calculated with the relation (35) using the exact RWA ($ay_l(a)$) and the approximated one ($ay_l^{\text{app}}(a)$). The agreement of $\theta^2(a)$ evaluated with $ay_l^{\text{app}}(a)$ with that using $ay_l(a)$ is rather good with 20% error at most. Compared with the experimental $\theta^2(a)$ given by the measured α -decay width Γ_α , it is found that the calculation reasonably describes the experimental decay width of $^8\text{Be}(0_1^+)$. Even for the case of the broad resonance of $^8\text{Be}(2_1^+)$, the α -decay width is reasonably described by the calculation.

D. ^9Li

We apply the present approximation to ^9Li and estimate the t -decay width of the $^6\text{He}+t$ cluster resonances predicted in the previous work [54]. The present approximation is applicable to the cluster channel $^6\text{He}(0^+)+t$ where the orbital

TABLE III: The experimental and theoretical values of the dimensionless reduced width $\theta^2(a)$ of the $^{16}\text{O}+\alpha$ channel of ^{20}Ne at the channel radius $a = 5$ and $a = 6$ fm. The experimental $\theta^2(a)$ is calculated using the measured α decay widths [76]. The theoretical values are those of the RGM and GCM calculations taken from Refs. [61, 63]. The energy E (MeV) measured from the threshold is also listed.

	Exp.				Γ_α (keV)
	E	$\theta^2(a)$			
		$a = 5$	$a = 6$		
$^{20}\text{Ne}(0_1^+)$	−4.73				
$^{20}\text{Ne}(2_1^+)$	−3.1				
$^{20}\text{Ne}(4_1^+)$	−0.48				
$^{20}\text{Ne}(6_1^+)$	4.05	0.073(17)	0.0103(23)	0.110(25)	
$^{20}\text{Ne}(8_1^+)$	7.22	0.0095(27)	0.00094(27)	0.035(10)	
$^{20}\text{Ne}(1_1^-)$	1.06	1.04	0.32	0.028	
$^{20}\text{Ne}(3_1^-)$	2.43	0.97	0.28	8.2	
$^{20}\text{Ne}(5_1^-)$	5.53	1.08	0.32	145	
$^{20}\text{Ne}(7_1^-)$	10.64	0.24	0.07	110	
		$a = 6$	$a = 7$		
$^{20}\text{Ne}(0_{\text{hn}}^+)$	4	>0.39	>0.37	>800	
$^{20}\text{Ne}(2_{\text{hn}}^+)$	4.3	~0.52	~0.43	~800	
$^{20}\text{Ne}(4_{\text{hn}}^+)$	6.06	0.23	0.17	350	
		RGM [63]		GCM [61]	
	E	$\theta^2(a)$		E	
		$a = 5$	$a = 6$	$\theta^2(a)$	
				$a = 6$	
$^{20}\text{Ne}(0_1^+)$	−4.26			−3.9	0.057
$^{20}\text{Ne}(2_1^+)$	−3.25			−2.72	0.052
$^{20}\text{Ne}(4_1^+)$	−0.94			0.05	0.041
$^{20}\text{Ne}(6_1^+)$	2.52	0.49	0.054	3.73	0.024
$^{20}\text{Ne}(8_1^+)$	6.77	0.16	0.015	9.86	0.006
$^{20}\text{Ne}(1_1^-)$	0.3	2.2	0.57	−0.3	0.267
$^{20}\text{Ne}(3_1^-)$	1.98	2.23	0.58	1.69	0.265
$^{20}\text{Ne}(5_1^-)$	5.08	2.28	0.6	5.3	0.271
$^{20}\text{Ne}(7_1^-)$	9.89	2.28	0.61	9.91	0.298
$^{20}\text{Ne}(0_{\text{hn}}^+)$				3.01	0.604
$^{20}\text{Ne}(2_{\text{hn}}^+)$				3.77	0.578
$^{20}\text{Ne}(4_{\text{hn}}^+)$				5.46	0.501

angular momentum of the inter-cluster motion is decoupled from the internal spins of clusters. ^9Li wave functions are obtained by the $^6\text{He}+t$ cluster-GCM calculation in the same way as Ref. [54]. Namely, the $^6\text{He}+t$ -cluster BB wave functions with $S_k = 1, \dots, 8$ fm are superposed to describe $J^\pi = 1/2^-, 3/2^-, 5/2^-,$ and $7/2^-$ states of ^9Li . Practically, the cluster wave functions are described by the linear combination of AMD wave functions with specific configurations as done in the previous work. The ^6He cluster is expressed by the H.O. shell-model configurations. The configuration mixing in the major shell is taken into account, and all $^6\text{He}(0^+)$ and $^6\text{He}(2^+)$ states in the $(0s)^4(0p)^2$ configurations are incorporated. In the ground state, $^6\text{He}(0_1^+)$, obtained in the p -shell, $(p_{3/2})^2$ and $(p_{1/2})^2$ configurations are mixed. Because of the configuration mixing in the ^6He cluster, it is not easy to get the RGM norm kernel and to calculate the exact RWA of the $^6\text{He}(0_1^+)+t$ cluster channel. Instead, we calculate the overlap norm of the ^9Li wave function with the $^6\text{He}(0_1^+)+t$ -cluster BB wave function at a certain channel radius $S_k = a$ and obtain the approximated value $ay_i^{\text{aPP}}(a)$ of the RWA to discuss the t -decay width of the cluster resonance states.

The interaction and width parameters are those used in the previous work. The interaction is Volkov No.2 with $m = 0.60, b = h = 0.125$ supplemented by the spin-orbit term of the G3RS force with the strength $u_I = -u_{II} = 1600$ MeV, which is adjusted to reproduce the energy spectra of ^{10}Be with the $^6\text{He}+\alpha$ cluster-GCM calculation. The width parameter $\nu = 0.235 \text{ fm}^{-2}$ is used. In the present work, all K states are mixed in the cluster-GCM calculation while

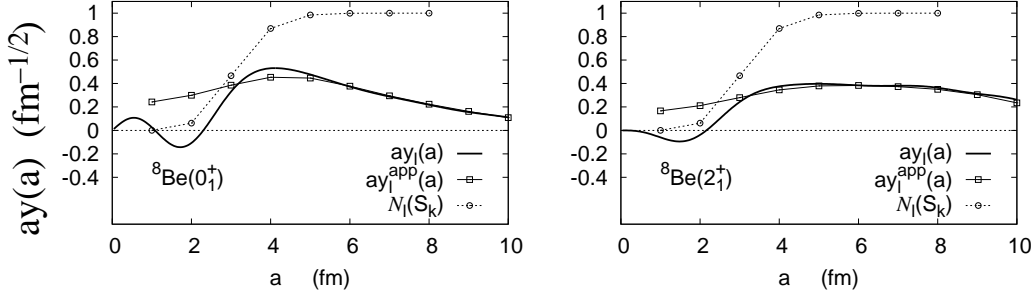


FIG. 7: The approximated RWA $ay_l^{\text{app}}(a)$ and the exact $ry_l(a)$ of the $\alpha+\alpha$ channel in the 0_1^+ and 2_1^+ states of ^8Be obtained by the cluster-GCM calculation using the Volkov No.2 force ($m = 0.60$) and the width parameter $\nu = 0.25 \text{ fm}^{-2}$. The allowedness factor $N_l(S_k = a)$, which indicates the weakness of the antisymmetrization effect between clusters, in the projected BB wave function $\Phi_{\text{BB}}^{J\pi}(S_k)$ with $S_k = a$ is also shown.

TABLE IV: Calculated energies E (MeV) measured from the 2α threshold and dimensionless reduced width $\theta^2(a)$ of the $\alpha+\alpha$ channel for $^8\text{Be}(0_1^+)$ and $^8\text{Be}(2_1^+)$ obtained by the cluster-GCM calculation compared with the experimental data [77]. The calculated $\theta^2(a)$ is evaluated with the relation 35 using the exact RWA $ay_l(a)$ and the approximated one $ay_l^{\text{app}}(a)$. The channel radius $a = 5, 6$, and 7 fm are chosen.

	cluster-GCM						
	E	$\theta^2(a)$			$\theta^2(a)$		
		exact			approx.		
		$a = 5$	$a = 6$	$a = 7$	$a = 5$	$a = 6$	$a = 7$
$^8\text{Be}(0_1^+)$	0.18	0.33	0.28	0.20	0.38	0.28	0.19
$^8\text{Be}(2_1^+)$	2.37	0.24	0.29	0.33	0.26	0.30	0.34
	Exp.						
	E	$\theta^2(a)$			$\Gamma_\alpha(\text{keV})$		
		$a = 5$	$a = 6$	$a = 7$			
$^8\text{Be}(0_1^+)$	0.092	0.27	0.19	0.14	0.00557		
$^8\text{Be}(2_1^+)$	3.122	0.50	0.47	0.48	1513		

K was truncated as $|K| \leq 3/2$ in the previous calculation. For $J^\pi = 5/2^-$ and $7/2^-$ states, the lower energy spectra is changed by the mixing of high K states, but it does not change the feature of the $^6\text{He}+t$ resonance states near the threshold.

We here briefly explain the structure of the ground and excited states of ^9Li obtained by the $^6\text{He}+t$ cluster-GCM calculation. For more details of the structure of ^9Li , the reader is referred to Ref. [54]. The energies E measured from the $^6\text{He}+t$ threshold energy are plotted as function of the spin $J(J+1)$ in Fig. 8. $^9\text{Li}(1/2_1^-)$, $^9\text{Li}(3/2_1^-)$, $^9\text{Li}(5/2_2^-)$, $^9\text{Li}(7/2_1^-)$ are regarded as members of the ground band. In the highly excited states near the threshold, $^9\text{Li}(1/2_2^-)$, $^9\text{Li}(3/2_3^-)$, $^9\text{Li}(5/2_3^-)$, $^9\text{Li}(7/2_2^-)$ show the ^6He and t resonance feature and they are regarded as the $^6\text{He}+t$ cluster resonances as discussed in the previous work. $^9\text{Li}(3/2_2^-)$ and $^9\text{Li}(5/2_1^-)$ are shell model-like states given by p -shell configurations having dominantly the $K = 3/2$ ($L_z = 2$) component. $^9\text{Li}(1/2_3^-)$, $^9\text{Li}(3/2_4^-)$, $^9\text{Li}(5/2_5^-)$, and $^9\text{Li}(7/2_3^-)$ are considered to be non-resonance states strongly coupling with $^6\text{He}+t$ continuum states.

Using the overlap norm of the ^9Li wave function with the $^6\text{He}(0_1^+)+t$ -cluster BB wave function at a certain channel radius $S_k = a$, we calculate the approximated value $ay_l^{\text{app}}(a)$ of the RWA and estimate the partial decay width for the $^6\text{He}(0_1^+)+t$ channel of the resonances near the threshold. In the present $^6\text{He}+t$ cluster-GCM calculation, the channel coupling is incorporated, and therefore, $^6\text{He}(0^+)+t$ and $^6\text{He}(2^+)+t$ cluster channels are coupled in ^9Li wave functions. However, the present approximation of the RWA is applicable only for the case that the relative angular momentum l does not couple with the intrinsic angular-momenta of clusters. Therefore, we can analyze only the $^6\text{He}(0_1^+)+t$ -cluster component and discuss the RWA and the partial decay width of this channel. As mentioned before, the cluster wave function for the ground state $^6\text{He}(0_1^+)$ is the linear combination of H.O. $(p_{3/2})^2$ and $(p_{1/2})^2$ coupling to totally zero angular momentum. In the $^6\text{He}(0_1^+)+t$ -cluster BB wave function with the distance parameter S_k , which is expressed

by the linear combination of AMD wave functions, this corresponds to the sub-projection (spin-parity projection of the subsystem ${}^6\text{He}$) and the state mixing in the ${}^6\text{He}$ cluster.

We first determine the applicable region of the present approximation of the RWA by excluding the channel radius $S_k = a$ with the strong antisymmetrization effect. From the calculated allowedness factor $\mathcal{N}_l(S_k)$ of $l = 1$ for $J^\pi = 1/2^-$ and $J^\pi = 3/2^-$ states and that of $l = 3$ for $J^\pi = 5/2^-$ and $J^\pi = 7/2^-$ states shown in Fig. 9, we find that the region $S_k \geq 3$ fm satisfies the criterion $\mathcal{N}_l(S_k) \geq 0.6$ and consider this region as the applicable region of the present approximation.

The calculated $ay_l^{\text{app}}(a)$ for the ${}^6\text{He}(0_1^+) + t$ channel in the cluster-GCM wave functions of the ground and excited states of ${}^9\text{Li}$ is shown in Fig. 10. In the ground band members, the amplitude at $a = 3 \sim 4$ fm indicates the relatively large probability of the t cluster at the surface in ${}^9\text{Li}(1/2_1^-)$ and ${}^9\text{Li}(3/2_1^-)$ compared with ${}^9\text{Li}(5/2_2^-)$ and ${}^9\text{Li}(7/2_1^-)$. The surface probability of t is suppressed in the high spin $7/2_1^-$ states, maybe, because of the centrifugal barrier. For ${}^9\text{Li}(5/2_2^-)$, $ay_l^{\text{app}}(a)$ shows a long tail of the inter-cluster wave function reflecting the energy position E near the threshold. In ${}^9\text{Li}(3/2_2^-)$ and ${}^9\text{Li}(5/2_1^-)$, $ay_l^{\text{app}}(a)$ is very small. This is consistent with the fact that these states are dominated by the $K^\pi = 3/2^-$ states and mainly contain the excited cluster component ${}^6\text{He}(2^+)$ rather than ${}^6\text{He}(0^+)$. ${}^9\text{Li}(1/2_2^-)$, ${}^9\text{Li}(3/2_3^-)$, ${}^9\text{Li}(5/2_3^-)$, and ${}^9\text{Li}(7/2_2^-)$ show the peak structure of the RWA around $a = 6$ fm indicating the resonance feature of developed ${}^6\text{He}$ and t clusters. The smaller RWA values in ${}^9\text{Li}(5/2_3^-)$ and ${}^9\text{Li}(7/2_2^-)$ than those in ${}^9\text{Li}(1/2_2^-)$ and ${}^9\text{Li}(3/2_3^-)$ are understood by the coupling with the ${}^6\text{He}(2^+) + t$ with the $l = 1$ wave of relative motion because of the alignment of the ${}^6\text{He}$ cluster in high spin states. In non-resonant continuum states, ${}^9\text{Li}(1/2_3^-)$, ${}^9\text{Li}(3/2_4^-)$, ${}^9\text{Li}(5/2_5^-)$, ${}^9\text{Li}(7/2_3^-)$, $ay_l^{\text{app}}(a)$ is no longer confined in the finite region.

We estimate the partial width of ${}^6\text{He}(0_1^+) + t$ decay with the relation (35) using the calculated $ay_l^{\text{app}}(a)$. Experimentally, the ${}^6\text{He} + t$ resonances have not been observed yet. We here use the theoretical values of the decay energy E in the estimation of the decay width. The calculated dimensionless reduced width $\theta^2(a)$ and the decay width Γ are listed in Table V. We choose the channel radius $a = 3, 4$, and 5 fm for the ground band and $a = 5, 6$, and 7 fm for the cluster resonances. The calculated partial decay width $\Gamma_{{}^6\text{He}(0_1^+) \rightarrow t}$ of ${}^9\text{Li}(5/2_2^-)$ is as small as 10 keV order because this state is the shell model state with less cluster development. For the cluster resonances, ${}^9\text{Li}(1/2_2^-)$ and ${}^9\text{Li}(3/2_3^-)$, the present result suggests the width $\Gamma_{{}^6\text{He}(0_1^+) \rightarrow t}$ of the order 1 MeV, which is consistent with the width estimation of the pseudo potential method in the previous work. Much smaller partial widths are suggested for ${}^9\text{Li}(5/2_3^-)$ and ${}^9\text{Li}(7/2_2^-)$ because ${}^6\text{He}(0_1^+) + t$ component is suppressed originating in the coupling with the $l = 1$ -wave ${}^6\text{He}(2^+) + t$ channel due to the ${}^6\text{He}$ alignment. In the present calculation, the ${}^6\text{He}(2_1^+) + t$ channel is open for ${}^9\text{Li}(5/2_3^-)$ and ${}^9\text{Li}(7/2_2^-)$ while it is closed for ${}^9\text{Li}(1/2_2^-)$ and ${}^9\text{Li}(3/2_3^-)$. For the total t -decay width of ${}^9\text{Li}(5/2_3^-)$ and ${}^9\text{Li}(7/2_2^-)$, it is necessary to estimate also the ${}^6\text{He}(2_1^+) + t$ decay width. However, since the application of the present approximation is restricted only for the spinless cluster case, it is a future problem to be solved.

In the present calculation, we assume the H.O. p -shell configuration for the ${}^6\text{He}$ cluster. Although such the H.O. ${}^6\text{He}$ wave function is too simple to describe the details of the ${}^6\text{He}$ structure, it may have a significant overlap with more sophisticated ${}^6\text{He}$ wave function and therefore the present calculation may be useful for order estimation.

It should be also noted that the n decay is important to discuss the total width of ${}^9\text{Li}$ states. The n decay channel is omitted in the present ${}^6\text{He} + t$ cluster-GCM calculation. However, for the ${}^6\text{He} + t$ cluster resonances, ${}^9\text{Li}(1/2_2^-)$, ${}^9\text{Li}(3/2_3^-)$, ${}^9\text{Li}(5/2_3^-)$, and ${}^9\text{Li}(7/2_2^-)$, the n decay might be suppressed because the ${}^6\text{He} + t$ cluster structure develops so well that those cluster states have small overlap with the ${}^8\text{Li} + n$ component and hence it is naively expected that the t decay can be the dominant decay channel. Of course, it is not the case if the energy position of the ${}^6\text{He} + t$ cluster states is low enough to close the t decay channel.

VI. SUMMARY AND OUTLOOKS

We proposed a method to approximately evaluate the RWA of the spinless two-body cluster channel using the overlap with the BB cluster wave function at a channel radius. The applicability of the approximation was tested for ${}^{16}\text{O} + \alpha({}^{20}\text{Ne})$ and $\alpha + \alpha({}^8\text{Be})$ systems. It was found that the approximated RWA for the cluster states near the threshold energy is in good agreement with the exact RWA in the outer region. Using the approximated RWA, we estimated the α -decay width in the bound state approximation and showed that the method is useful to discuss the α -decay width of resonance states.

We applied the present method to ${}^9\text{Li}$, and estimate the partial decay width of the ${}^6\text{He}(0_1^+) + t$ channel for the cluster resonance states near the threshold energy. The present result suggests the significant ${}^6\text{He}(0_1^+) + t$ component in ${}^9\text{Li}(1/2_2^-)$ and ${}^9\text{Li}(3/2_2^-)$ at $1 \sim 2$ MeV above the threshold with the t -decay width of the order 1 MeV.

In the present work, we apply the present method to systems consisting of simple cluster wave functions given by H.O. configurations. The proposed method is based on the norm overlap with a cluster wave function localized around a certain distance S_k which can be rather easily calculated than the exact inter-cluster wave function. Therefore, the

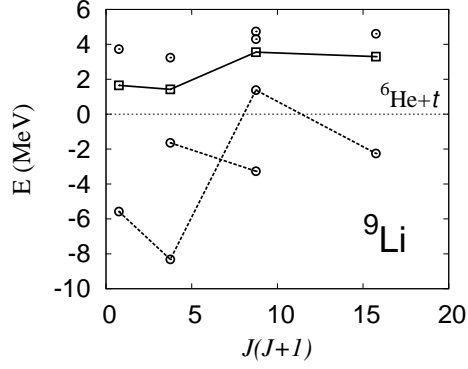


FIG. 8: Calculated energy spectra of negative-parity states in ${}^9\text{Li}$ obtained by the ${}^6\text{He}+t$ cluster-GCM calculation using the Volkov No.2 force ($m = 0.60, b = h = 0.125$) supplemented by the spin-orbit term of the G3RS force ($u_I = -u_{II} = 1600$ MeV). The energies E of ${}^9\text{Li}$ states measured from the ${}^6\text{He}+t$ threshold are plotted as functions of the spin $J(J+1)$.

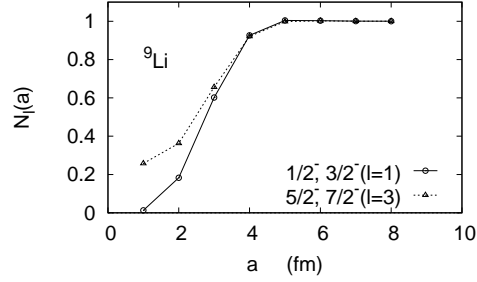


FIG. 9: The allowedness factor $\mathcal{N}_l(S_k = a)$, which indicates the weakness antisymmetrization effect between clusters, in the ${}^6\text{He}+t$ -cluster wave function with $S_k = a$.

present method is efficient and it is applicable to systems consisting of more complicated cluster wave functions. For instance, it may be feasible to evaluate the α decay width of the ${}^{10}\text{Be}+\alpha$ -cluster states, which has been theoretically suggested in excited states of ${}^{14}\text{C}$ [38]. Moreover, application to heavier mass nuclei is promising for systematic study of α -cluster states in a wide mass number region.

Acknowledgments

The authors would like to thank Dr. Ogata and Dr. Fukui for fruitful discussions. The computational calculations of this work were performed by using the supercomputers at YITP. This work was supported by JSPS KAKENHI Grant Numbers 22540275, 25887049, 25800124, 26400270.

-
- [1] S. Ohkubo *et al.*, Prog. Theor. Phys. Suppl. **132**, 1 (1998).
 - [2] W. von Oertzen, M. Freer and Y. Kanada-En'yo, Phys. Rep. **432**, 43 (2006).
 - [3] Y. Kanada-En'yo and H. Horiuchi, Prog. Theor. Phys. Suppl. **142**, 205 (2001); Y. Kanada-En'yo M. Kimura and H. Horiuchi, C. R. Physique **4**, 497 (2003); Y. Kanada-En'yo, M. Kimura and A. Ono, PTEP **2012** (2012) 01A202.

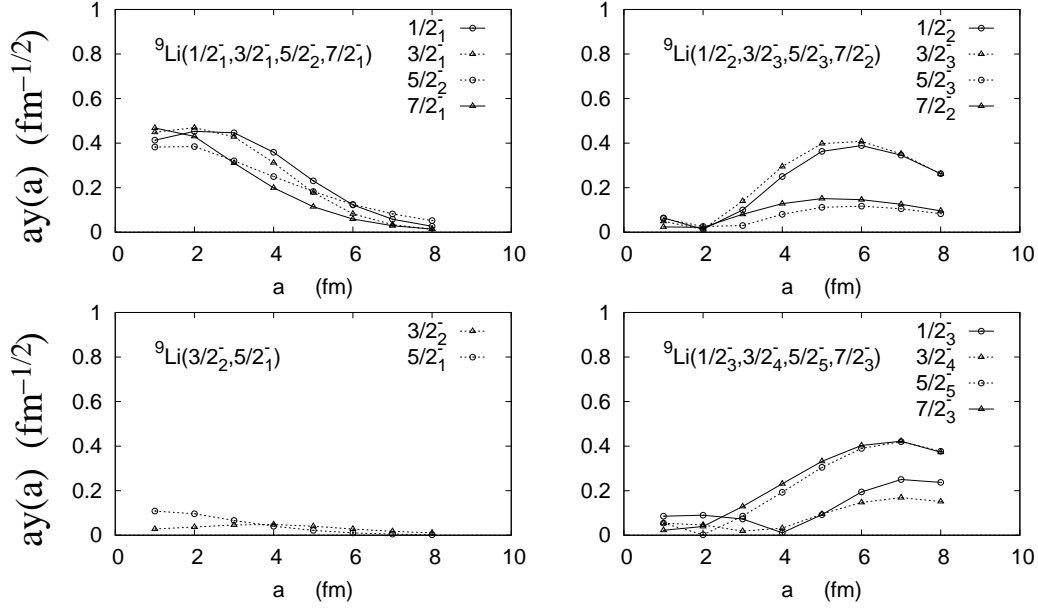


FIG. 10: The approximated RWA $ay_l^{\text{app}}(a)$ of the ${}^6\text{He}(0_1^+)-t$ channel in ${}^9\text{Li}$ obtained by the ${}^6\text{He}+t$ cluster-GCM calculation. Upper left panel: $ay_l^{\text{app}}(a)$ for the ground band members: ${}^9\text{Li}(1/2_1^-)$, ${}^9\text{Li}(3/2_1^-)$, ${}^9\text{Li}(5/2_2^-)$, and ${}^9\text{Li}(7/2_1^-)$. Lower left panel: that for the $K = 3/2^-$ band members, ${}^9\text{Li}(5/2_1^-)$ and ${}^9\text{Li}(3/2_2^-)$. Upper right panel: that for the ${}^6\text{He}+t$ resonance states, ${}^9\text{Li}(1/2_2^-)$, ${}^9\text{Li}(3/2_3^-)$, ${}^9\text{Li}(5/2_3^-)$, and ${}^9\text{Li}(7/2_2^-)$. Lower right panel: that ${}^9\text{Li}(1/2_3^-)$, ${}^9\text{Li}(3/2_4^-)$, ${}^9\text{Li}(5/2_5^-)$, ${}^9\text{Li}(7/2_3^-)$ which are regarded as non-resonant states strongly coupling with continuum states.

TABLE V: The calculated partial decay width and dimensionless reduced width $\theta^2(a)$ for the ${}^6\text{He}(0_1^+)+t$ decay of ${}^9\text{Li}$ evaluated with $ay_l^{\text{app}}(a)$. The channel radius $a = 3, 4$, and 5 fm are chosen for the ground band members and $a = 5, 6$, and 7 fm are chosen for the ${}^6\text{He}+t$ resonance states near the threshold. The energy E (MeV) measured from the ${}^6\text{He}+t$ threshold is also listed.

	E	$\theta^2(a)$ approx.			$\Gamma_{{}^6\text{He}(0_1^+)-t}$ (MeV)		
		$a = 3$	$a = 4$	$a = 5$	$a = 3$	$a = 4$	$a = 5$
${}^9\text{Li}(1/2_1^-)$	-5.58	0.20	0.17	0.089			
${}^9\text{Li}(3/2_1^-)$	-8.32	0.18	0.13	0.053			
${}^9\text{Li}(5/2_2^-)$	1.38	0.10	0.083	0.055	0.002	0.005	0.009
${}^9\text{Li}(7/2_1^-)$	-2.25	0.10	0.053	0.022			
		$a = 5$	$a = 6$	$a = 7$	$a = 5$	$a = 6$	$a = 7$
${}^9\text{Li}(1/2_2^-)$	1.65	0.22	0.30	0.28	0.68	0.88	0.75
${}^9\text{Li}(3/2_3^-)$	1.42	0.26	0.33	0.29	0.70	0.84	0.68
${}^9\text{Li}(5/2_3^-)$	3.55	0.021	0.027	0.026	0.045	0.074	0.077
${}^9\text{Li}(7/2_2^-)$	3.30	0.038	0.043	0.037	0.071	0.10	0.10

- [4] H. Horiuchi, K. Ikeda, and K. Katō "Recent Developments in Nuclear Cluster Physics" Prog. Theor. Phys. Suppl. **192**, 1 (2012).
- [5] K. Ikeda, N. Tagikawa, and H. Horiuchi, Prog. Theor. Phys. Suppl. extra number, 464 (1968).
- [6] K. Ikeda *et al.*, Prog. Theor. Phys. Suppl. **52**, 1 (1972).
- [7] M. Seya, M. Kohnno, and S. Nagata, Prog. Theor. Phys. **65**, 204 (1981).
- [8] W. von Oertzen, Z. Phys. A **354**, 37 (1996); **357**, 355 (1997).
- [9] W. von Oertzen, Nuovo Cimento **110**, 895 (1997).
- [10] K. Arai, Y. Ogawa, Y. Suzuki and K. Varga, Phys. Rev. C **54**, 132 (1996).

- [11] A. Dote, H. Horiuchi and Y. Kanada-En'yo, Phys. Rev. C **56**, 1844 (1997).
- [12] K. Fujimura, D. Baye, P. Descouvemont, Y. Suzuki and K. Varga, Phys. Rev. C **59**, 817 (1999).
- [13] Y. Kanada-En'yo, H. Horiuchi and A. Doté, Phys. Rev. C **60**, 064304 (1999).
- [14] N. Itagaki and S. Okabe, Phys. Rev. C **61**, 044306 (2000); N. Itagaki, S. Okabe and K. Ikeda, Phys. Rev. C **62**, 034301 (2000).
- [15] Y. Ogawa, K. Arai, Y. Suzuki and K. Varga, Nucl. Phys. **A673**, 122 (2000).
- [16] K. Arai, Y. Ogawa, Y. Suzuki, and K. Varga, Prog. Theor. Phys. Suppl. **142**, 97 (2001).
- [17] P. Descouvemont, Nucl. Phys. A **699**, 463 (2002).
- [18] Y. Kanada-En'yo, Phys. Rev. C **66**, 011303 (2002).
- [19] Y. Kanada-En'yo and H. Horiuchi, Phys. Rev. C **68**, 014319 (2003).
- [20] M. Ito, K. Kato and K. Ikeda, Phys. Lett. B **588**, 43 (2004).
- [21] K. Arai, Phys. Rev. C **69**, 014309 (2004).
- [22] M. Ito, Phys. Lett. B **636**, 293 (2006).
- [23] J. C. Pei and F. R. Xu, Phys. Lett. B **650**, 224 (2007) [nucl-th/0612025].
- [24] M. Ito, N. Itagaki, H. Sakurai and K. Ikeda, Phys. Rev. Lett. **100**, 182502 (2008).
- [25] N. Soić *et al.*, Europhys. Lett. **34**, 7 (1996).
- [26] M. Freer, *et al.*, Phys. Rev. Lett. **82**, 1383 (1999); M. Freer, *et al.*, Phys. Rev. C **63**, 034301 (2001).
- [27] J. A. Liendo, N. Curtis, D. D. Caussyn, N. R. Fletcher and T. Kurtukian-Nieto, Phys. Rev. C **65**, 034317 (2002).
- [28] A. Saito, *et al.*, Nucl. Phys. **A738**, 337 (2004).
- [29] N. Curtis *et al.*, Phys. Rev. C **70**, 014305 (2004).
- [30] M. Milin *et al.*, Nucl. Phys. **A753**, 263 (2005).
- [31] M. Freer *et al.*, Phys. Rev. Lett. **96**, 042501 (2006).
- [32] H. G. Bohlen, T. Dorsch, T. Kokalova, W. von Oertzen, C. Schulz and C. Wheldon, Phys. Rev. C **75**, 054604 (2007).
- [33] N. Curtis, N. I. Ashwood, M. Freer, T. Munoz-Britton, C. Wheldon, V. A. Ziman, S. Brown and W. N. Catford *et al.*, J. Phys. G **36**, 015108 (2009).
- [34] N. Soic, M. Freer, L. Donadille, N. M. Clarke, P. J. Leask, W. N. Catford, K. L. Jones and D. Mahboub *et al.*, Phys. Rev. C **68**, 014321 (2003).
- [35] W. von Oertzen *et al.*, Eur. Phys. J. **A 21**, 193 (2004).
- [36] D. L. Price, M. Freer, N. I. Ashwood, N. M. Clarke, N. Curtis, L. Giot, V. Lima and P. M. Ewan *et al.*, Phys. Rev. C **75**, 014305 (2007).
- [37] P. J. Haigh, N. I. Ashwood, T. Bloxham, N. Curtis, M. Freer, P. McEwan, D. Price and V. Ziman *et al.*, Phys. Rev. C **78**, 014319 (2008).
- [38] T. Suhara and Y. Kanada-En'yo, Phys. Rev. C **82**, 044301 (2010).
- [39] P. Descouvemont and D. Baye, Phys. Rev. C **31**, 2274 (1985).
- [40] M. Gai, M. Ruscev, A. C. Hayes, J. F. Ennis, R. Keddy, E. C. Schloemer, S. M. Sterbenz and D. A. Bromley, Phys. Rev. Lett. **50**, 239 (1983).
- [41] M. Gai, R. Keddy, D. A. Bromley, J. W. Olness and E. K. Warburton, Phys. Rev. C **36**, 1256 (1987).
- [42] N. Furutachi, S. Oryu, M. Kimura, A. Dote and Y. Kanada-En'yo, Prog. Theor. Phys. **119**, 403 (2008).
- [43] C. Fu, V. Z. Goldberg, G. V. Rogachev, G. Tabacaru, G. G. Chubarian, B. Skorodumov, M. McCleskey and Y. Zhai *et al.*, Phys. Rev. C **77**, 064314 (2008).
- [44] E. D. Johnson, G. V. Rogachev, V. Z. Goldberg, S. Brown, D. Robson, A. M. Crisp, P. D. Cottle and C. Fu *et al.*, Eur. Phys. J. A **42**, 135 (2009).
- [45] W. von Oertzen *et al.*, Eur. Phys. J. **A 43**, 17 (2010).
- [46] N. Curtis, D. D. Caussyn, C. Chandler, M. W. Cooper, N. R. Fletcher, R. W. Laird and J. Pavan, Phys. Rev. C **66**, 024315 (2002).
- [47] N. I. Ashwood, M. Freer, S. Ahmed, N. M. Clarke, N. Curtis, P. McEwan, C. J. Metelko and V. Ziman *et al.*, J. Phys. G **32**, 463 (2006).
- [48] S. Yildiz, M. Freer, N. Soic, S. Ahmed, N. I. Ashwood, N. M. Clarke, N. Curtis and B. R. Fulton *et al.*, Phys. Rev. C **73**, 034601 (2006).
- [49] W. Scholz, P. Neogy, K. Bethge and R. Middleton, Phys. Rev. C **6**, 893 (1972).
- [50] P. Descouvemont, Phys. Rev. C **38**, 2397 (1988).
- [51] M. Kimura, Phys. Rev. C **75**, 034312 (2007).
- [52] G. V. Rogachev, V. Z. Goldberg, T. Lonnroth, W. H. Trzaska, S. A. Fayans, K. -M. Kallman, J. J. Kolata and M. Mutterer *et al.*, Phys. Rev. C **64**, 051302 (2001).
- [53] V. Z. Goldberg, G. V. Rogachev, W. H. Trzaska, J. J. Kolata, A. Andreyev, C. Angulo, M. J. G. Borge and S. Cherubini *et al.*, Phys. Rev. C **69**, 024602 (2004).
- [54] Y. Kanada-En'yo and T. Suhara, Phys. Rev. C **85**, 024303 (2012).
- [55] J. A. Wheeler, Phys. Rev. **52** 1083 (1937); J. A. Wheeler, Phys. Rev. **52** 1107 (1937).
- [56] K. Wildermuth, Th. Kanellopoulos, Nucl. Phys., **7**, 150 (1958); K. Wildermuth, Th. Kanellopoulos, Nucl. Phys., **9**, 449 (1958/1959).
- [57] D. L. Hill and J. A. Wheeler, Phys. Rev. **89**, 1102 (1953); J. J. Griffin and J. A. Wheeler, Phys. Rev. **108**, 311 (1957).
- [58] D. M. Brink, International School of Physics "Enrico Fermi", XXXVI, p. 247 (1966).
- [59] R. Tamagaki, H. Tanaka, Prog. Theor. Phys. **34**, 191 (1965); R. Tamagaki, Prog. Theor. Phys. Suppl. Extra Number, 242 (1968); J. Hiura and R. Tamagaki, Prog. Theor. Phys. Suppl. **52**, 25 (1972).

- [60] W. Sünkel, K. Milderuth, Phys. Lett. **B41**, 439 (1972).
- [61] F. Nemoto and H. Bandō, Prog. Theor. Phys. **47**, 1210 (1971).
- [62] T. Matsuse, M. Kamimura, and Y. Fukushima, Prog. Theor. Phys. **49**, 1765 (1973).
- [63] T. Matsuse, M. Kamimura, and Y. Fukushima, Prog. Theor. Phys. **53**, 706 (1975).
- [64] K. Ikeda *et al.*, Prog. Theor. Phys. Suppl. **62**, 1 (1977).
- [65] Y. Kanada-En'yo and H. Horiuchi, Prog. Theor. Phys. **93**, 115 (1995).
- [66] Y. Kanada-En'yo, H. Horiuchi and A. Ono, Phys. Rev. C **52**, 628 (1995); Y. Kanada-En'yo and H. Horiuchi, Phys. Rev. C **52**, 647 (1995).
- [67] Y. Kanada-En'yo, Phys. Rev. Lett. **81**, 5291 (1998).
- [68] H. Feldmeier, K. Bieler and J. Schnack, Nucl. Phys. A **586**, 493 (1995).
- [69] H. Feldmeier and J. Schnack, Rev. Mod. Phys. **72**, 655 (2000).
- [70] R. Roth, T. Neff, H. Hergert and H. Feldmeier, Nucl. Phys. A **745**, 3 (2004).
- [71] T. Neff, Phys. Rev. Lett. **106**, 042502 (2011).
- [72] K. Varga, Y. Suzuki and R. G. Lovas, Nucl. Phys. A **571**, 447 (1994).
- [73] M. Kimura and H. Horiuchi, Phys. Rev. C **69**, 051304 (2004).
- [74] A. B. Volkov, Nucl. Phys. **74**, 33 (1965).
- [75] N. Yamaguchi, T. Kasahara, S. Nagata and Y. Akaishi, *Prog. Theor. Phys.* **62**, 1018 (1979); R. Tamagaki, *Prog. Theor. Phys.* **39**, 91 (1968).
- [76] D. R. Tilley, C. Cheves, J. Kelley, S. Raman, H. Weller, Nucl. Phys. A **636**, 249 (1993).
- [77] J. H. Kelley, J. L.=Godwin, C. G. Sheu, *et al.*, Nucl. Phys. A **745**, 155 (2004).